AN ABSTRACT OF THE THESIS OF

Nicholas Wehmann for the degree of Master of Science in Radiation Health Physics presented on January 19, 2018.

Title: Locating and Quantifying Contamination Deposited by Radiation Puncture Wounds.

Abstract approved:

_____

David M. Hamby

Internal dosimetry models show a representation of how radionuclides move through the body. This study takes a look at radiation wounds by modelling a puncture wound to the hand using Microshield software. An analysis of these models provides a triangulation method that could be used to investigate wound characteristics, as well as radionuclide deposition within the wound. This triangulation method provides a better understanding of what a wound looks like under the skin, which is important for the appropriate response and treatment for radiation wounds.

Locating and Quantifying Contamination Deposited by Radiation Puncture Wounds

by
Nicholas Wehmann

A THESIS

submitted to

Oregon State University

in partial fulfillment of
the requirements for the
degree of

Master of Science

Presented January 19, 2018
Commencement June 2018

Master of Science thesis of Nicholas Wehmann presented on January 19, 2018

APPROVED:

Major Professor, representing Radiation Health Physics

Head of the School of Nuclear Sciences and Engineering

Dean of the Graduate School

I understand that my thesis will become part of the permanent collection of Oregon State University libraries. My signature below authorizes release of my thesis to any reader upon request.

Nicholas Wehmann, Author

ACKNOWLEDGEMENTS

I would like to thank my family, especially my father Ron Wehmann, for all the support they have provided for me over the tough journey it has been to achieve this academic milestone. I owe my major advisor, Dr. Hamby, enormously for all the support and knowledge he provided to me throughout my graduate school experience. His willingness to answer questions and challenge me to think critically about subject matter made this research possible. I would also like to thank the staff and faculty of the School of Nuclear Sciences and Engineering for helping me to get over all the hurdles and difficult challenges this experience has brought. Additionally, the completion of this project would not have been possible without the support and understanding of all the staff members of Naval Surface Warfare Center, Crane Division, specifically the members of the radiation safety team, and Dr. Matt Halstead. A special thanks goes to the staff of the In-Vitro Radioassay Research Facility in Richland, WA. Without the expert knowledge of Tim Lynch, Eugene Carbaugh, and Cheryl Antonio, this project would not have been possible. Finally, I want to thank my friends for being there to support me with their kindness and understanding, as well as their willingness to work with me as sounding boards for my ideas and theories.

TABLE OF CONTENTS

Page

LIST OF FIGURES

Figure Page

LIST OF TABLES

Table Page

LIST OF EQUATIONS

Chapter 1: Introduction and Background

Many facilities across the United States use radioactive nuclides to perform a variety of tasks. These tasks can range from decontamination and decommissioning of old nuclear sites to the use of medical nuclides in a hospital setting. As with any industry, accidents can and do still occur in the nuclear field. In settings where radiation contamination is present, these accidents can lead to wounds, such as punctures or scrapes. When a worker receives a wound in this type of working environment it is possible for the radioactive contaminants to be deposited inside the body, using the open wound as an access point.

A radiation wound, for the purposes of this paper, is a wound that is incurred in an area where radioactive contamination is present and which may contain residual radioactive contaminants. This can result in radioactive material being deposited inside the wound. Once the radioactivity has entered the body via the broken skin caused by the wound, there are several potential response options. Before any of these options can be employed, more information about the potential contamination of the wound is needed.

A complication of treatment for radiation puncture wounds is the lack of knowledge about the wound itself. Once a worker has received a puncture wound, the only information that is readily available can be seen on the surface of the skin at the entry point. To aid physicians in any potential excision scenarios, more detailed information should be obtained. Combining a collimator and multiple counts from different locations around a wound

could provide a sort of three dimensional look at the wound, and where the activity is located inside it. The creation of a three dimensional model of a wound would tell physicians what the general shape of the wound is under the skin, for example it is straight down or if it curves to one side or another, and aid them in surgical excision of contaminated tissue while minimizing removal/damage of healthy uncontaminated tissues.

When a worker first receives a puncture wound in such an environment, it is often unclear if the wound has any contamination. Before treatment options such as chelation therapy or excision are utilized, it is important to obtain an initial radiation count to provide either a positive or negative indication regarding the presence of radionuclides (Hickman, 2006). These initial counts can be performed in a variety of settings, whether that is in the field or in a local health physics office is dependent on the specific situation. Both sodium iodide (NaI) and high purity germanium (HPGe) detectors can be used to obtain this type of count. The need to keep high purity germanium detectors at cold temperatures can reduce their effectiveness as portable wound counters since they would no longer be quick and easy to transport.

Once the initial count has confirmed the presence of radionuclides in a wound, additional counts can be performed to reveal more information about what the wound looks like and where in the wound the radionuclides are concentrated.

Wounds can occur anywhere on the body, from the foot and lower calf all the way up the top of the head (Lynch & Carbaugh, 2017). For this research, the wound model was based on a puncture wound to the hand. Specifically, a puncture in between the second and third metacarpals at the proximal end of the second and third phalanges. The wound itself was modeled after a puncture one might receive from a standard Philips head screwdriver.

Two main techniques have been utilized in the field of wound counting. Wounds have been counted in a variety of settings, from out in the field using portable counting equipment like the instrument used at Lawrence Livermore National Laboratory, which is a sodium iodide detector combined with a Canberra NaI InSpector™ and a laptop computer (Hickman, 2006). This technique (Figure 1.1) can detect radiation present in the wound, however in order to keep the system portable, there is little to no shielding which means that background radiation can have a significant impact on counts. Without shielding, external sources of radiation such as naturally occurring isotopes or cosmic radiation can have an impact on the count. These external factors can result in higher counts that can conceal what is actually present in the wound.

Figure 1.1: LLNL Portable Wound Counter (Hickman, 2006)

Contrasting this type of counting environment is one of the facilities used at the Department of Energy Hanford Site. The In Vivo Radio-bioassay and Research Facility (IVRRF), is a facility in Richland, Washington that is used to perform in vivo radiation counts on workers at the Hanford site (Figure 1.2). For wound counting this facility maintains a portable wound counter similar to the device used at Lawrence Livermore, as well as high purity germanium detectors that are kept in well shielded rooms. These detectors are used primarily for lung and whole body counts on workers, but are also used for wound counting. This type of equipment setup is more accurate for determining activity in a wound than portable wound counters. Since this setup has more shielding to reduce background radiation counts, it

would be the ideal setup to add in additional techniques that would yield more information about the radiation wound.

Figure 1.2: Counting Cell at the IVRRF (Alikhani, 2014)

The composition of the shielding varies since the facility houses three different rooms. However, the rooms are constructed from pre-World War II materials. These materials are used to minimize any background radiation that could skew the counts. By adding shielding, sources of radiation such as naturally occurring nuclides or cosmic radiation have less of an impact on wound counts. This is beneficial because it allows for a better estimate of how much contamination and what nuclides may be present in a wound. For example, one room uses the armor plating from a battleship (the U.S.S. Indiana) as part of its shielding. When possible, workers are counted in one of these well shielded rooms with reproducible counting geometry. In addition, the counting equipment in these rooms automatically subtracts the

background. Overnight background counts are regularly collected at this facility to keep the background correction accurate.

Accounting for background radiation at the facility allows for more accurate counts to be performed. The background counts allow the facility to take into account any nuclides that may be present in the soil beneath the building, or even in the materials or equipment present inside the counting cell.

The wound counting processes and procedures used at the IVRRF were used as the basis of planning the work done for this thesis. The process for wound counting at the site begins once the injured worker has arrived at the IVRRF. The counts may be performed quickly after the wound is incurred up to a few hours or days afterwards. The timeline is dependent on what kind of care is needed for the wound. The treatment of the physical injury is the first priority, and takes precedence over any radioactive contamination (Hall & Giaccia, 2012). In preparation for the worker's arrival, the germanium detector(s) that will be used to count the wound will have a thin layer of Saran-wrap placed over the counting face of the detector. This is to prevent the detector from being contaminated by any biological or radiological hazards without significantly impacting the accuracy of the count. The plastic wrapped face is then centered above the wound and placed in close proximity to the skin for the count to be performed. Currently the staff at the IVRRF use these counts as a positive or negative confirmation of activity, and to obtain a rough estimate of how much activity has been deposited/remains in the wound

area. However, these counts do not constitute the final determination of deposited activity.

In addition to using well shielded facilities to perform the counting, other techniques could be applied to increase the understanding of contamination deposited in a wound. One such technique is the combination of collimators and multiple counts. In this case collimators are made of a material with a small hole punched through it that will help shield the detector from radiation except for the location of the hole. The collimators help to identify areas where the activity has been deposited, since they essentially reduce the counting area to the size of the hole in the collimator material. By moving the opening in the collimator to various points around the center of the wound the activity could be triangulated. This can be combined with multiple counts from the top, bottom, and sides of a wound to understand the geometry of the wound, and the deposition of material inside it.

In some puncture wound cases, it is possible for the instrument causing the puncture to enter the body at an angle, or to curve once it is under the skin. From the perspective of a person looking at the exterior of the wound it would be nearly impossible to determine if the wound is a straight line, and if not what shape the wound is under the skin. However, applying a combination of a collimating material and multiple counting geometries could reveal more information about the wound, and what lies under the skin.

NCRP Wound Model

In 2007, the US National Council on Radiation Protection and Measurements (NCRP), published Report No. 156. This report contained a compartment model for internal dosimetry following the accidental uptake of radionuclides through a wound (Ishigure, 2009) [Figure 1.3]. The model created by the NCRP has five main compartments. The compartments are abbreviated: Soluble (SOL), Colloid and Intermediate State (CIS), Particles, Aggregates and Bound State (PABS), Trapped Particles and Aggregates (TPA), and Fragments (FRG) (Ishigure, 2009). These compartments are used to describe the physical and chemical properties of any radionuclide that may be deposited in a wound. The radionuclide can be directly input into four of the main compartments, TPA is the only compartment that cannot receive direct input from the "accidental injection". The injected radionuclides will transition from one compartment to another, with the transfer rates being based on individual element properties, until the nuclide reaches the blood. Once the injected material has reached the blood, it acts as it would if it had

been directly injected into the bloodstream (Ishigure, 2009).

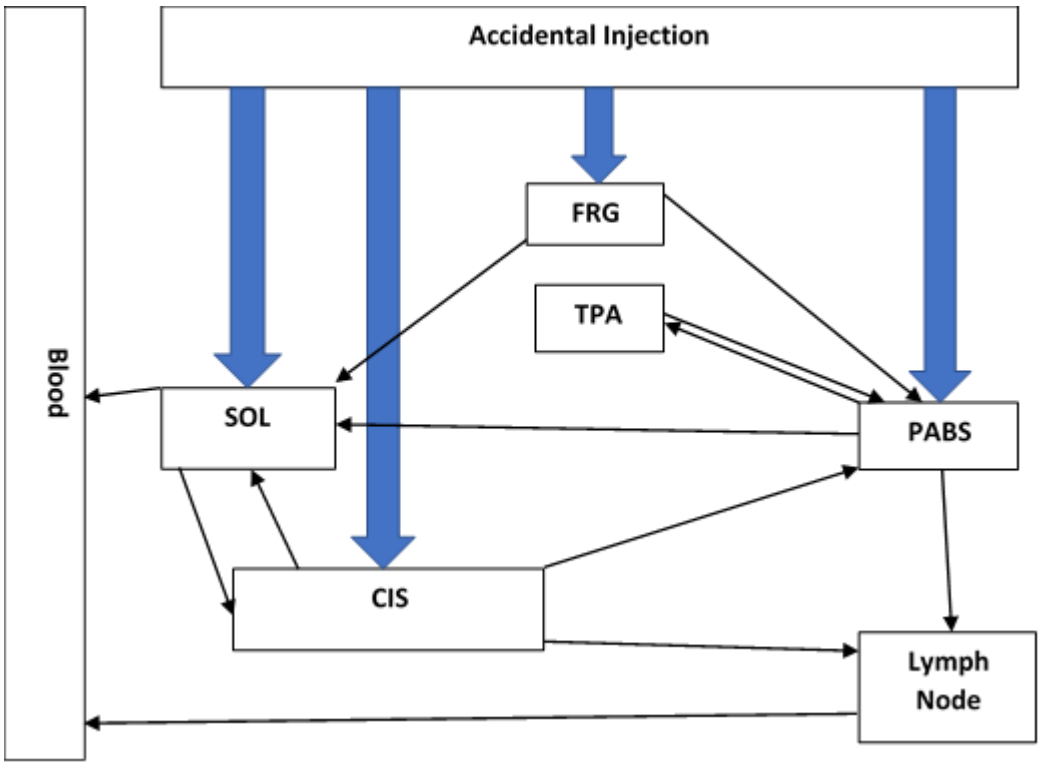

Figure 1.3: Compartmental Description of the NCRP Wound Model

The default transfer rates for this compartment model can be seen in Table 1.1 (Ishigure, 2009). The Table only lists values that are non-zero. The first four columns in the Table describe soluble substances. In this section, these substances are divided into: weak, moderate, strong, or avid solubility. Depending on the chemical properties, multiple classes can be assigned. The exact classification of a substance in the soluble classes is based on how what fraction of the initially injected activity remains at the site twenty-four hours after the initial deposition, and the rate at which this retained fraction was removed from the site (Ishigure, 2009). The NCRP wound model initially focused primarily on puncture wounds, which is what makes it of relevance to this work. As a result, the transfer rates for this model are based on material

that was injected through a puncture wound (Ishigure, 2009).

Transfer	Transfer rate (d^{-1})						
	Weak	Moderate	Strong	Avid	Colloid	Particle	Fragment
Soluble→Blood	45	45	0.67	7.0	0.5	100	–
Soluble→CIS	20	30	0.6	30	2.5	–	–
CIS→Soluble	2.8	0.4	2.4×10^{-2}	3×10^{-2}	2.5×10^{-2}	–	–
CIS→PABS	0.25	6.5×10^{-2}	1.0×10^{-2}	10	5×10^{-2}	–	–
CIS→Lymph nodes	2×10^{-5}	2×10^{-5}	2×10^{-5}	2×10^{-5}	2×10^{-3}	–	–
PABS→Soluble	8×10^{-2}	2×10^{-2}	1.2×10^{-3}	5×10^{-3}	1.5×10^{-3}	2×10^{-4}	–
PABS→Lymph nodes	2×10^{-5}	2×10^{-5}	2×10^{-5}	2×10^{-5}	4×10^{-4}	3.6×10^{-3}	4×10^{-3}
PABS→TPA	–	–	–	–	–	4×10^{-2}	0.7
TPA→PABS	–	–	–	–	–	3.6×10^{-3}	5×10^{-4}
Lymph nodes→Blood	–	–	–	–	3×10^{-2}	6×10^{-4}	3×10^{-2}
Fragment→Soluble	–	–	–	–	–	–	–
Fragment→PABS	–	–	–	–	–	–	8×10^{-3}

Table 1.1: Default Transfer Rates for NCRP Wound Compartment Model

From looking at the compartment model from Report No. 156, a few different observations about the model can be made. One of the first realizations is that everything that is injected through the wound will, given enough time, end up in the blood stream. However, depending on the material classification and chemical properties, the time needed to arrive in the bloodstream will vary. From the values in Table 1.1, it can be seen that there are some compartments where injected material will accumulate. Primarily, the two locations where material will accumulate is in the lymph nodes, and in the trapped particles and aggregates compartment. The lymph node compartment has two routes in, one from PABS and the other from CIS, both inputs have relatively slow transfer rates compared to the soluble material. The lymph nodes have only one route out of the compartment where material

is transferred from the lymph nodes to blood. The materials that can be transferred out of the lymph nodes this way are the colloids, particles, and fragments (Ishigure, 2009). For the four soluble categories, values are given for their transfer into the lymph nodes, but no value is listed for their transfer out to blood. This is indicative of the soluble materials remaining in the lymph nodes indefinitely. The transfer rates for the colloids, particles, and fragments differ from the soluble materials. Colloids are removed from the lymph nodes at a slightly faster rate than the two input rates. Particles are removed at a slower rate. Fragments are removed at a slightly faster rate than their inputs.

The other compartment where materials can accumulate is the trapped particles and fragments (TPA) compartment. The TPA compartment has only one route in and one route out, and from Table 1.1 only accepts particles and fragments. Particles enter the compartment at a rate faster than they can be removed, however the larger difference occurs in the fragment portion. Fragments can be transferred significantly faster than they can be removed, which allows for a substantial buildup in this compartment.

Wound Physiology

The process of wound healing is a complex biological process that involves many different cells and cellular signals. The physiologic process of wound healing can be broken down into four main phases (Young & Mcnaught, 2011). The first phase of wound healing is called hemostasis. This is a near immediate response in which the body is trying to prevent

exsanguination (severe blood loss) by quickly constricting blood vessels, blood loss is also prevented by the formation of clots (Young & Mcnaught, 2011). The constricting of blood vessels is countered by other biological processes within minutes (Young & Mcnaught, 2011).

The second stage of wound physiology is inflammation. Inflammation occurs due to the body's immune response to a break in the primary protective barrier, the skin, which can allow foreign particles and pathogens into the body. In inflammation, cells such as neutrophils and macrophages make their way to the wound site. Once there, these cells have a few responses that can be used to remove bacteria and debris. For radiation wounds, the main concern is foreign particles inside the body. Both neutrophils and macrophages have phagocytotic abilities (Young & Mcnaught, 2011). This allows them to completely engulf and remove foreign cells and particles, though some particles injected into a wound site can be too large for removal (Young & Mcnaught, 2011). This is also the stage where any particles or fragments can become trapped in tissue, as seen in some radiation wound case studies (Carbaugh, Lynch, Antonio & Valle, 2010).

The next phase of wound healing is called proliferation. Proliferation is the stage where the body begins to repair itself. First, the blood vessels that were damaged or destroyed are rebuilt or repaired. Next, the body begins to construct a framework that will be used to repair the breach in the skin. Once the skin has started to grow back over the wound site, the wound begins to retract which reduces the area of tissue that needs to be healed (Young &

Mcnaught, 2011). The final stage of wound repair is remodeling. This phase can take up to two years to complete, and is the phase where scar tissue and normal skin tissue begin to form at the wound site.

Chapter 1.3: Photon Interactions and Dosimetry

Photons differ from other forms of radiation in that they are not charged, and carry no mass (Turner, 2007). As a result, photons do not lose energy at a fixed rate like charged particles do when they enter matter. When a photon enters a medium, the depth to which it will penetrate is determined by statistics and the probability that the photon will interact with the medium. This is dependent upon what specific medium the photon is entering and the energy of said photon. There are four types of interactions that a photon can undergo when interacting with matter (Turner, 2007).

The first type of interaction is the photoelectric effect. The photoelectric effect occurs when electrons are ejected from a surface as a result of energy absorption (Turner, 2007). In 1905, Einstein believed that the photoelectric effect occurred when an electron completely absorbs a single photon (Turner, 2007). Einstein also explained that the kinetic energy of the emitted photoelectron is equal to the energy of the incident photon minus the energy that is required to remove the electron from its orbital (Turner, 2007).

The next type of photon interaction with matter is the Compton effect, or Compton scattering. Compton scattering occurs when an incoming photon interacts with an electron in the target material. The photon transfers some of

its energy to the electron then oscillates with this newfound energy and emits radiation with an equal wavelength to that of the oscillations (Turner, 2007). After interaction, the incident photon is then scattered off the electron at an angle. The energy of the scattered photon is dependent on the initial energy of the photon, and the angle at which it is scattered. The photon can be scattered at any angle, while the electron is confined to be between zero and ninety degrees (Turner, 2007).

The third main type of photon interaction is pair production. In pair production, a photon is converted into an electron-positron pair when in the field of an atomic nucleus, it can also occur in the field of an atomic electron, however the probability of this occurring is much lower and more energy is required (Turner, 2007). This reaction has a threshold energy, below which the reaction cannot occur. The minimum energy required is 1.022 MeV, which is twice the mass of an electron at rest (Turner, 2007). This energy is required for the formation of the electron and positron pair. The opposite reaction then takes place when the positron and electron annihilate. The most likely occurrence from the annihilation reaction is the production of two .511 MeV photons travelling in opposite directions (Turner, 2007).

A final type of reaction is the photonuclear reaction. The probability for this type of reaction is significantly smaller than for the other three. The probability for photonuclear reactions being several orders of magnitude smaller than the sum of the probabilities for the other three reaction types (Turner, 2007).

To calculate the dose from exposure to photons, a few factors must be known. First, dose itself is energy absorbed per unit mass. The energy that is absorbed is dependent on three components. The first is the energy of the incident photon(s). This component describes how much energy is carried per photon. The second piece of the Equation is the flux. The flux describes how many photons are in a given area. The last piece that is needed is the interaction probability. The interaction probability is different for each medium, and describes the probability that a photon will undergo an interaction in said medium. Multiplying these three pieces together leaves units of energy/mass.

For photon dosimetry, there are multiple methods that can be used to calculate the dose to a human from photons. One such method is the point-kernel method, which allows for the calculation of dose at a single point, from a point source. This method is simple, and allows for a point to point dose calculation. Multiple point-kernel calculations can be done and then summed for multiple sources, or averaged over target volumes depending on the application.

For radiation puncture wounds, the most applicable model for dose calculations is that of a volume source. To calculate dose, Equation 1.1 used is:

$$D = flux * Energy_{gamma} * (\frac{\mu_{en}}{\rho})_{medium}$$

Equation 1.1 Dose Calculation

Where "$\mu_{en/\rho}$" is the photon interaction probability. This number is different for each medium.

To calculate the flux from a volume source, Equation 1.2 is used:

$$Flux = \frac{source\ strength}{\mu}(1 - e^{-\mu R})$$

Equation 1.2 Flux Calculation

Where "μ" is the linear attenuation coefficient, which represents "the quotient of the fraction of particles that experience interaction while traversing an incremental distance", and "R" is the distance from the center of the source to the point where dose is being evaluated.

Another important concept surrounding photon dosimetry is buildup factor. Buildup factor takes into account secondary radiations as well as scattered radiation (Baes, 2017). Because of this, calculations that include a buildup factor will be higher than calculations that only take primary radiations into account.

Chapter 2: Literature Review

Hickman (2006) described the various forms of error associated with the direct counting of radiation wounds. He found that there were four main sources of error with this type of counting, including: photon self-absorption, overlying tissue thickness, distribution in the wound, and counting errors (Hickman, 2006).

Jones and Saxby (1968) describe a plutonium wound that a worker received on the middle finger of the left hand. In their description of how the

wound was counted, several different techniques are mentioned. The activity in this case was located by using a variety of different "masking devices". Similarly, Jolly et al. (1972) also described the use of collimators to aid in the location of activity that was deposited inside a wound. The idea behind the use of collimators and other masking devices is to use the shielding to help find where the count rate is the highest. The locations with higher count rates are indicative of a larger deposition of radioactive material.

Another wound case was studied where the worker received a puncture wound to his left thumb. In this case the wound was investigated and the activity was mapped using a collimated detector (Bailey, Eckerman, & Townsend, 2003). The authors of this paper do not describe the specific counting procedures that allowed for the creation of the map of contamination. The map provided in the paper shows bars over different parts of the thumb where the wound was incurred, however this map does not describe the depth of the remaining radioactive contamination in the wound.

Carbaugh, Lynch, Antonio, & Valle (2010), looked back on twenty-four years of data on a radiation wound incurred at the Department of Energy Hanford site. The authors describe the follow up that was performed over the years for the injured employee. The procedures involved multiple external counts using high-purity germanium detectors with a standard counting geometry, as well as monitoring of excreta data (Carbaugh, Lynch, Antonio, & Valle, 2010). However, there was no use of a collimator for this work.

An analysis of a separate case where a worker received a cut on his right index finger was performed by Schadilov, Belesokhov, & Levina (2010). The analysis of this wound was done with a solid-state germanium detector at a whole body counting facility. The worker received a surgical intervention which reduced the activity in the wound significantly. That led the authors to conclude that a large portion of the activity in the wound was due to large particles (Schadilov, Belesokhov, & Levina, 2010). What makes this case more complicated is that the worker had received previous radiation wounds with confirmed activity in the same location of the body as the most recent wound that was incurred in October of 2006. The report indicates that the previous wounds were treated and reduced to be indistinguishable from background, however no collimator was used in the more recent wound and the authors acknowledge that detection levels may have played a role in how much activity was discovered.

In this case the collimators (Figure 2.1) would be plates of materials with small holes in them. The small holes would allow photons from a small area of tissue to be detected by the radiation detector, while attenuating those photons that were coming from other areas of the wound. By moving this plate around to different locations near the wound site, a better picture of where the activity was deposited could be obtained.

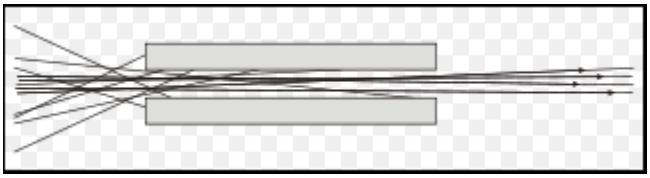

Figure 2.1: Collimator Example (Photo from Wikipedia)

Another paper looked at radioactively contaminated wounds in an entirely different manner. Weber, Doyle-Eisele, Seilkp, & Guilmette (2012) worked on developing a biokinetic model for internal exposures using rats. In this experiment, rats were injected with cobalt-60, and their urine and feces were collected and analyzed for the presence of cobalt. While the rats were alive, bioassay data was used to determine the intake and retention of cobalt for each specimen.

Griffiths, Coudert, Renault, Wilk, & Van der Meeren (2014) also utilized rats to study radiation contamination in wounds. In this study the rats had activity placed inside a surgically created wound, and then received treatments such as DTPA and surgical excision. In this experiment, the initial activity in the wounds was determined using a sodium iodide detector. The rats were sedated to reduce movement, and their wounds were placed within the area of the detector, however no collimator or multiple counting geometry was used.

A paper by Ishigure (2009) discusses the implementation of the biokinetic and dosimetric models that were released by the U.S. National Council on Radiation Protection and Measurements in 2007. This article brings up important points about the potential contamination that can be found in radiation wounds. The NCRP wound model has seven categories of contaminants (Ishigure, 2009). Four of these categories are soluble materials, while the remaining three are not. Of interest in this research were the non-soluble forms such as particles and fragments. According to Ishigure (2009)

these forms can be formed from even soluble nuclides if an exterior matrix is available. They found this to mean that almost every isotope can form a particle or a fragment that can then be deposited inside a wound.

A paper by Kirby et al. (1977) worked on analyzing soil from the Nevada Test Site for americium and plutonium. In their work, they used a method of rotating their soil samples during counts that were performed by a high purity germanium detector. They then used these results to create depth distribution contours for their soil samples. This technique is something that could be applied to radiation wounds. Rather than rotating the sample, or in this case the injured worker, the detectors could be moved and multiple counts performed to help create a depth distribution of deposited activity.

Chapter 3: Materials and Methods

For this project, a simple wound model was constructed using the Microshield software. An important note about Microshield is that it only accounts for photons, not other types of radiation such as alpha or beta. This software allows for the creation of a source of radiation as well as several shielding materials to be placed around the source. The source can be generated in a variety of geometries, and the shielding materials can come from a pre-made library within the software or they can be custom made based on the density and the composition of the desired material. The two main materials that needed to be simulated in Microshield were tissue and bone. The tissue was simulated using water, since the two materials have similar densities, and since water was already defined as a material in the

software package. To simulate bone, the information was input manually into the computer. The density of bone varies between 1.24 g/cm^3 for trabecular bone and 1.19 g/cm^3 for cortical bone (Tassani, Ohman, Baruffaldi, Baleani &Viceconti, 2010). For the purposes of these models, the density of cortical bone was used. Cortical bone was chosen because it is the type of bone that comprises long bones, and even though they are physically short, the metacarpals of the hand are physiologically long boned (Vorvick, 2015). The models also assume that the bone is of the same composition all the way through. The mineral hydroxyapatite ($Ca_{10}(PO_4)_6(OH)_2$) was used to obtain information about the chemical composition of bone (Cember & Johnson, 2009).

Before the wound model could be created, a location on the body had to be chosen so that accurate dimensions could be obtained. The staff of the IVRRF provided information about where on the body they had seen radiation wounds occur (Lynch & Carbaugh, personal communication, 2017). Ultimately, the location that was chosen for the model was a wound to the hand. Specifically, a wound between the second and third metacarpal bones evenly spaced between the proximal joint of the second and third phalanges and the second and third metacarpal.

This location was chosen because as seen in the literature, the hand is a common place for wounds to occur. Additionally, the staff of the IVRRF have performed studies on wounds to the hand, and were able to provide some guidance into the matter. The specific location on the hand was chosen

because that is where it is likely someone will receive an injury from an accident with a hand-held tool or object. This location was also chosen because it fit a case study that was performed by the IVRRF staff where a worker was holding a bottle in one hand and working on it with a tool when the tool punctured the bottle, the worker's glove, and the skin of the hand (Carbaugh, Lynch, Antonio, & Valle, 2010). All of these factors were combined to determine a location for the hypothetical wound for this research.

Measurements regarding the thickness of tissue and the dimensions of bone were collected from the author's left hand using a digital caliper (Figure 3.2). The caliper came from the manufacturer with an accuracy value of +/- 0.03mm, and a resolution of 0.01mm. The measurement of tissue thickness was done with care to ensure that the tissue was not compressed, thus representing an accurate tissue thickness to be used in the model.

Figure 3.1: Digital Caliper

Again, from communications with the health physics staff of the IVRRF (Lynch & Carbaugh, personal communication, 2017), a specific tool for the infliction of the radiation wound was selected. The instrument chosen for this project was a Philips head screwdriver that was obtained from a standard home repair kit. The diameter of the shaft of the screw driver was measured using the same digital caliper that was used to obtain data from the hand.

For the source, another tool contained in the Microshield software was used. The software contains a tool called "source inference". This tool allows for a spectrum of energies to be analyzed at the exposure points chosen by the user. For this research, the default settings for source inference were used, which resulted in the use of twenty-five photon energies. The selected energies ranged from 0.015 MeV to 15.0 MeV. The energy range that was used was chosen because it covered a wide range of potential photon energies. The default settings on Microshield were used, and this ended the photon range at 15.0 MeV. While this would be a high energy photon, it was included to gain an understanding of a wide range of energies.

In the construction of the model, some assumptions were made. The first assumption is that the puncture made by the screwdriver was perfectly cylindrical all the way down. The second assumption is that the activity that was on the screwdriver was deposited homogenously throughout the wound. The third assumption is that the tissue and bone surrounding the puncture site were of the same respective densities all the way through.

Three different models were constructed in Microshield. The first model (Figure 3.4) utilized a cylindrical source with a rectangular shield on the right-hand side. The shield was given the density of bone and thickness of the second metacarpal (personal measurement). On the other side of the shield, five exposure points were placed in a vertical line, with the first exposure point being placed in a position equivalent to the dorsal side of the hand, and the last exposure point being placed on the palmar side with the remaining exposure points being spaced equally between the first and the last. This model provided a side view of the puncture wound from top to bottom.

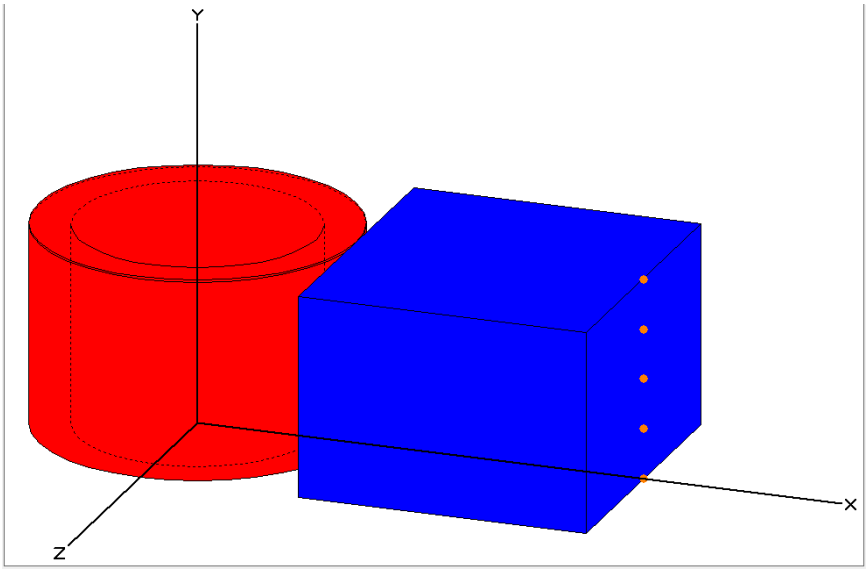

Figure 3.2: puncture wound with bone side shield and side exposure points (model 1)

The second model (Figure 3.5) that was created used a cylindrical source with a side shield that encompassed the source. There was also a small layer on top of both cylinders to simulate the outermost layer of skin that was needed to place the exposure points on top of the cylinder to meet requirements set by Microshield. The top and side shields were given the

density value for tissue. The width of the shield was equal to the thickness of tissue that would remain between the outer edges of the puncture and the bones of the second and third metacarpals (personal measurement). The exposure points for this case started centered directly over the top of the puncture and radiated outward towards the farthest edge of tissue before the bone began in evenly spaced increments.

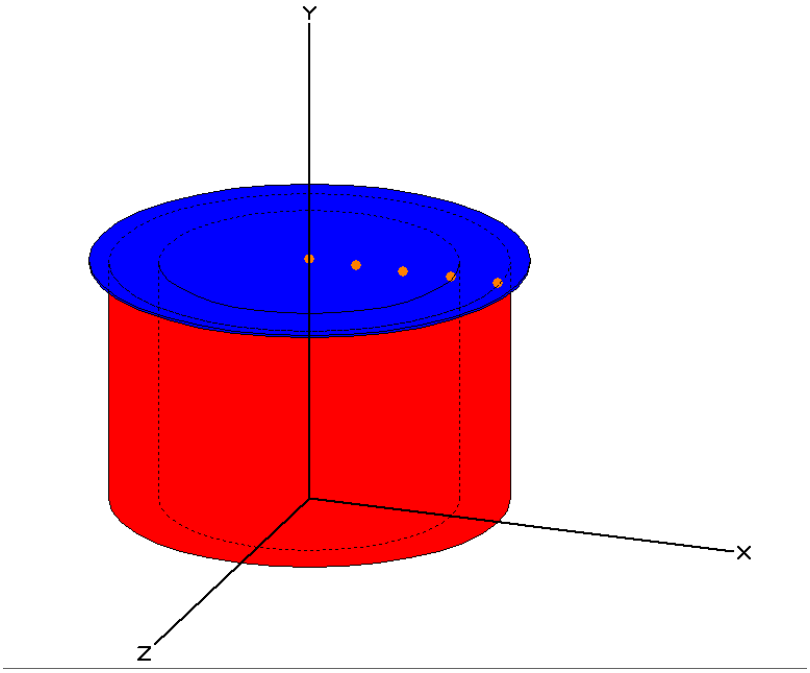

Figure 3.3: Puncture wound with top exposure points (Model 2)

A third model (Figure 3.6) was created in a similar fashion to the second model. A cylindrical source with an encompassing shield, with a thin layer of shielding on top of both cylinders. The dimensions of the shields and their density values were the same as the second model. For this setup however, only three exposure points were used. Only three exposure points were used, because that was all that was needed to confirm the hypothesis that all three would report the same results. All three exposure points were placed

on top of the source and surrounding shielding, though their X, Y, and Z coordinates were different. The three points were placed approximately equal distances from the center of the puncture, and were arranged in such a fashion as to form a sort of arc. The intent with this placement was to test a method for triangulating any activity that was deposited in the simulated wound.

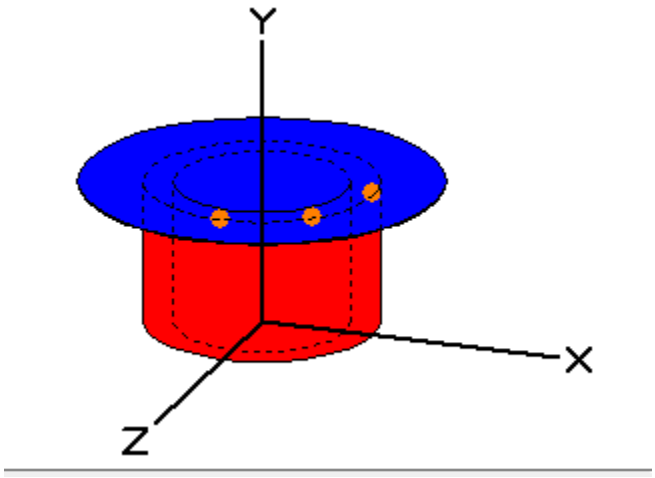

Figure 3.4: Model 3 (Top Triangulation)

Each of the models created for this project utilized multiple exposure points. This allowed for the simulation of many different counting geometries at the same time and reduced the time needed to collect the data. The data was reported by Microshield in a Table, giving fluence rate with and without buildup in units of MeV/cm^2/second, as well as exposure rate with and without buildup in milliroentgen per hour. For data analysis, only the exposure rate with buildup was used. The exposure rate with buildup factor was used because in radiation wound scenarios, the secondary and scattered radiations are important for dosimetry and exposure assessments. The

numbers reported by Microshield for exposure with buildup were exported into Microsoft Excel, where all data calculations were performed.

To determine the source activity within the wound, conversion factors were created for each model. The default settings in Microshield use a source activity of one becquerel. Taking this exposure rate received by each exposure point and dividing it by the activity over the course of one-hour results in the ability to convert the exposure for each model into source activity. The time frame of one-hour was chosen because that is the typical time that a wound is counted at a facility, such as the IVRRF in Richland, WA. The full hour count time is not necessarily required in all cases. It was chosen based on working experience at an internal dosimetry facility. Other counting times could be chosen based on the situation and needs of the users.

The steps to implement this type of counting technique are as follows. First, a worker would have to sustain a wound in an environment with radiation contamination, possibly in decontamination work, or in a glove box type setting. The employee would then report the incident and be sent to the local counting facility or health physics office for confirmation of contamination. Ideally, the facility would have a similar level of shielding as the IVRRF (described above) to reduce background counts. Now, the wound occurred in the same location as in the models, and in the same geometrical orientation, the following procedures would be used to accumulate the various counts.

First, counts from the top side of the wound should be collected. This will help determine what the wound geometry looks like. This is done by using a collimated detector. The collimator should be small relative to the approximate size of the wound to get a better determination of specific activity deposition. Counts should be collected first at the center of the wound, and then moved outwards towards the inner edge of the second metacarpal. If the exposure rates drop off, then it is an indicator that the wound is indeed straight up and down. To confirm this, the same process should be followed from the center of the wound to the inner edge of the third metacarpal. These two measurements would help to confirm or deny the curvature of a wound under the skin in the "X" direction. To gain an understanding of the "Y" curvature, the same process would be followed, but moving from the center of the wound towards the knuckles of the hand, and then again from the center of the wound towards the wrist.

This could also be achieved by using a slightly different methodology. As is shown in the third model, the exposure points could be moved around the center of the wound in larger and larger radii to provide information about whether the wound curves under the skin, and if so where on this curve the deposited activity lies.

To locate activity in the "Z" direction, the same steps would be applied, for a totally vertical wound. If either the "X" or "Y" measurements indicated a curvature to the wound, then a different methodology would be applied. To account for the curvature of the wound, counts would be

accumulated in the same fashion, just with an added slope to the line of movement for the counting equipment. The slope of this line would vary from case to case, depending on the severity of the curvature, and would most likely represent a line of best fit for the curvature of the wound.

Once these exposure measurements have been collected, the activity inside the wound can be back-calculated. As is shown later in this document, conversion factors for each case can be determined. These conversion factors, can then be applied to the measured exposure at each of the counting locations to provide the approximate activity deposited inside the wound.

Chapter 4: Modeling Results

In all three models, the results of the computer simulations produced graphs of exposure rate versus photon energy. For the first model, each of the exposure points reported exposure rates that were close together, shown in Figure 4.1. When the values from this trial were graphed, the lines for each exposure rate as a function of photon energy were indistinguishable from one another. This was as expected, since the exposure points were all similar distances away from the source with the shielding also remaining constant between points.

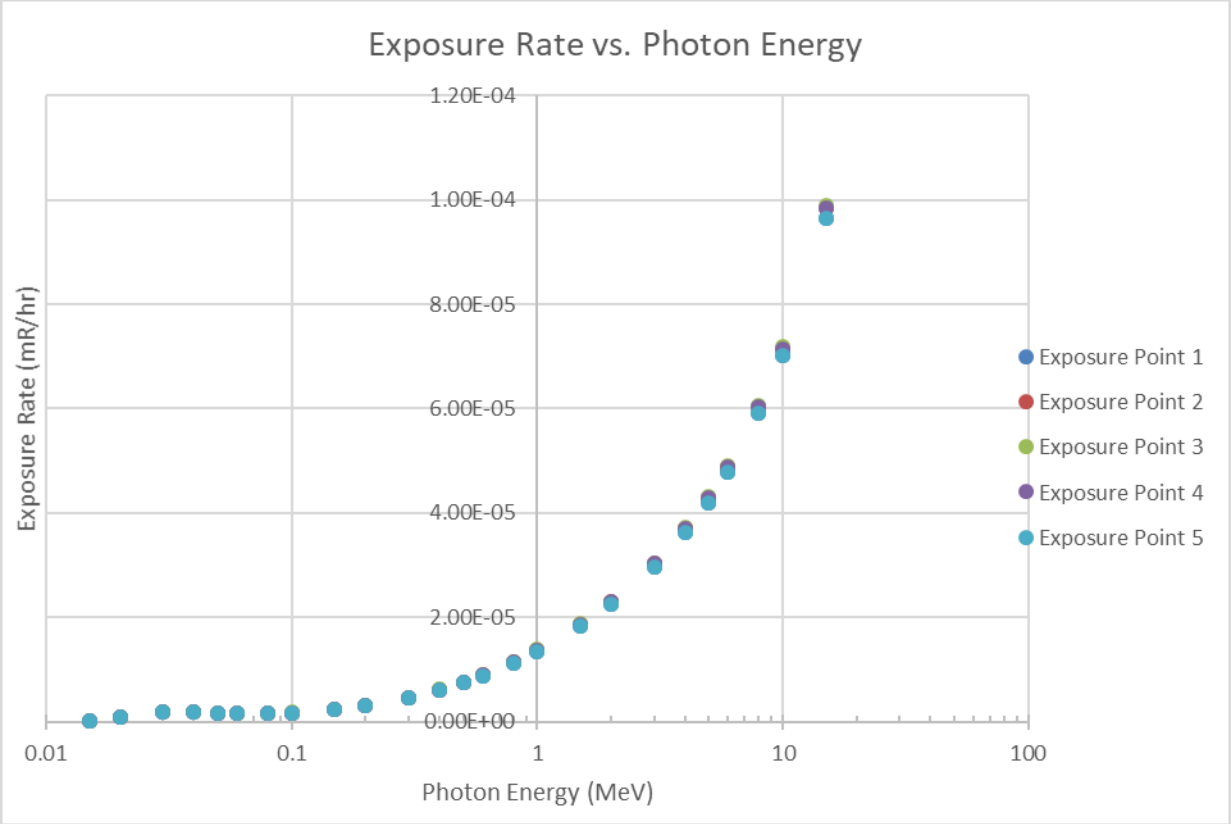

Figure 4.1: Exposure Rates for side bone shield and side exposure points (Model 1)

This is also the case for the third model (Figure 4.2) where the exposure points were arranged in an arc on top of the cylinder. This was expected for both cases.

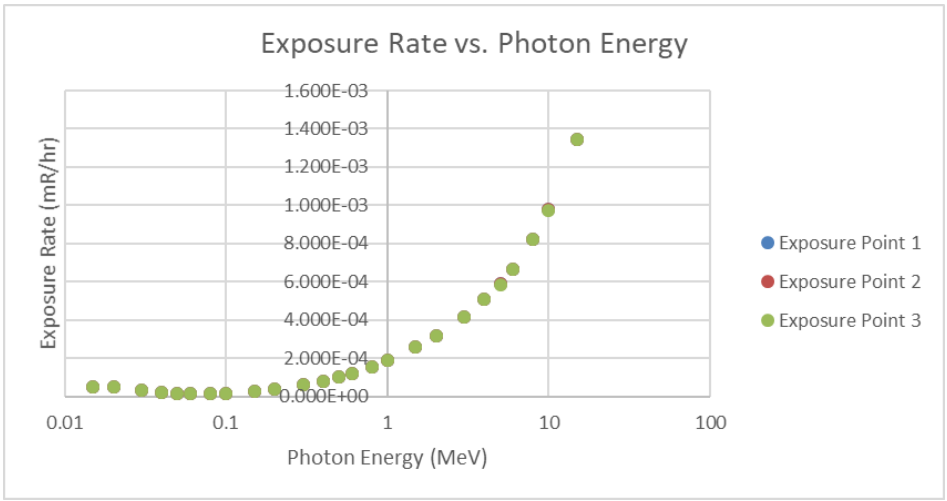

Figure 4.2: Exposure Rates for top exposure points in semi-circle (model 3)

For the second case where the exposure points were radiating outward from the center of the puncture in evenly spaced increments a different pattern was noted. In this model, as the dose points moved further from the center of the puncture, the exposure points reported lower exposure rates (Figure 4.3). This was also an expected occurrence due to the exposure points having different distances from the source.

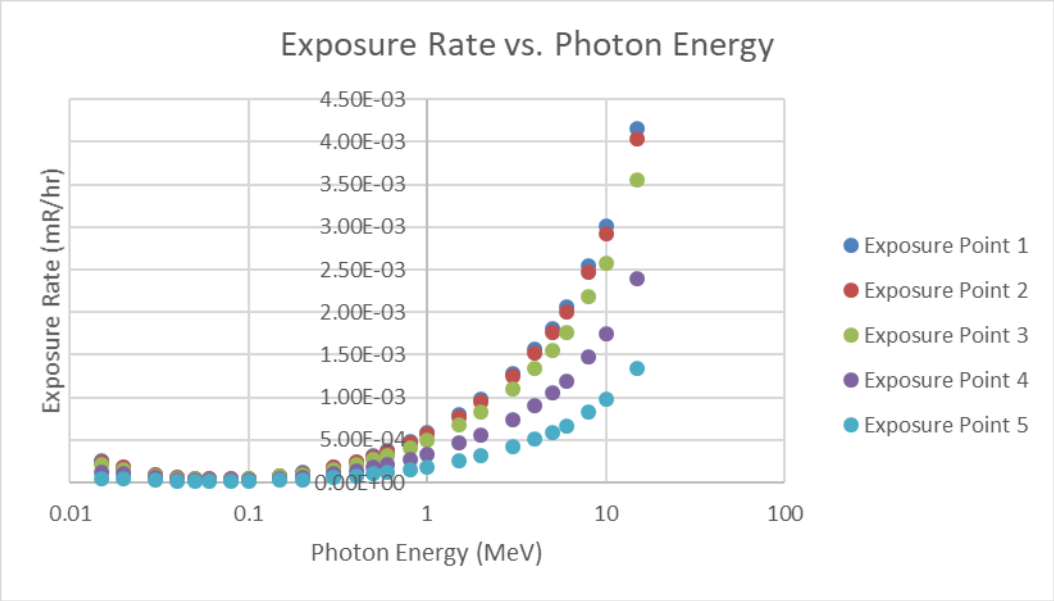

Figure 4.3: Exposure Rates for top exposure points arranged in linear fasion (Model 2)

Chapter 5: Discussion

While the results from each trial followed the expected patterns, there is still plenty of information that can be gleaned from these simulations. Each of the simulation setups followed the expected pattern of radiation attenuation in tissue. This helps to confirm that using multiple counting geometries can be successfully utilized as a technique to determine the location of radioactive contamination deposited in a wound. This works because the exposure points

show more or less activity when they are moved closer or further from the source of radiation, as seen in the second model where the exposure points radiated outward from the center of the puncture wound.

The first model that showed a side view of the wound can help determine not only relative depth of the deposited activity, but can also aid in the understanding of the wound itself. The depth of the deposited activity can be determined by taking counts from different sides of the wound. For example, with a wound to the hand in between the second and third metacarpals and the base of the fingers, one count could be taken from the outside edge of the second metacarpal, and a second count could be taken near the webbing between the fingers. With knowledge of tissue and bone density, the relative position of the activity in the wound can then be calculated from either side, giving a sort of X and Y coordinate. When an instrument punctures the skin, it is possible for the instrument causing the puncture to enter the body at an angle, or to change direction slightly once it is under the skin. While looking at the exterior of the wound it would be nearly impossible to determine the geometry of the wound under the skin.

This process could have impacts on wound dosimetry. First, it would allow for more accurate quantification of how much activity is initially in a wound. Second, it has implications for improving excision techniques. By knowing more accurately the depth of any deposited activity, a surgeon could more precisely remove the contaminated tissue, resulting in a lower dose over time for the patient.

The measurements from the first model indicate that if a wound was to curve under the surface of the skin that the reported exposure rate for some of the points would either increase or decrease depending on which way the wound was curved. If the wound curves away from the location where the count is being taken then the exposure rate will drop off. If the wound curves towards the counting location then the exposure rate will increase. By rotating the counting location by ninety degrees about the center of the puncture, a similar determination can be made for the second counting surface.

Looking at the data provided by the second and third models yields even more information about where activity is located in a wound. When the exposure points were evenly spaced from the center of the wound in a line towards the outer edge of tissue, there was a drop off in exposure rate as the points got further from the center of the puncture. The information that can be gained from these data shows that if the puncture is straight down then the exposure rate will drop off as the counting points get further from the center of the wound. If the wound is not straight down, i.e. curved or angled, then the exposure rates seen at the more outward points will be higher, and not as far off from the point that is centered directly above the wound entry point.

The data from the third model also illustrates this point. The third model had three exposure points arranged in an arc above the top shielding on the cylinder source. Each of these three points were approximately equally distant from the center of the wound, and each point reported approximately the same exposure rates. This method of arranging points would help in the

location of activity by providing a method of triangulation with which to pinpoint deposition in a wound.

These data sets show that the creation of a triangulation technique can be accomplished. To perform such a technique the following steps could be applied. First, the location of the wound would need to be analyzed. During the analysis, things such as the location of the wound relative to anatomical structures such as bone or cartilage should be noted so that the different material densities can be considered when performing counts. The next step would be to perform counts on one side of the wound. For example, using the experimental setup from this research, counting first from the back of the hand. Multiple counts from this side of the hand should be obtained. When performing these counts a collimator should be used to aid in pinpointing activity. For each count, the collimator should be moved to a different location, such that the hole in the collimator does not overlap with the previous counting area. If the collimator does overlap with the previous counting error, then an over-estimation of the deposited activity will occur. This step should be performed for each side of the wound including: top, bottom, and sides (as necessary). When the collimator is moved between counts, it can be moved as if an X/Y axis were place over the center of the wound. As the counting locations are moved across these axis, the counts can be recorded and then examined. From analyzing the counts, the shape of the wound, and relative deposition of activity can be determined.

If the puncture is straight down, then as the counting locations on the top and bottom get further from the center of the wound, a drop in total counts/exposure can be expected. However, if the counts stay relatively similar or get higher further from the center of the wound, this is an indication that the wound curves under the skin. The curve direction can be determined by using this same counting procedure.

The same procedure applied to the sides of a wound can yield similar data about the potential curvature of a wound. Additionally, if tissue thicknesses are taken into account for each side, the counts can be compared to find out which side the activity is closer to. Tissue and bone thicknesses will vary between each individual, if specific measurements surrounding a wound are obtained, then tissue attenuation can more accurately be accounted for. This information coupled with the data collected from the top and bottom counts can tell the operator relative depth of activity from the surface of the wound, and from the sides of the wound, allowing the activity to be triangulated.

For the determination of activity within a wound, the results provided by Microshield can be used to create a conversion factor. Tables of conversion factors for each of the simulated wounds can be seen in the appendix. The simulations that were ran in the software were done with an activity of one becquerel. By dividing this one becquerel by the exposure that was calculated for each point, a conversion factor of Bq/mR can be generated for each specific photon energy at each exposure point. These conversion

factors are represented in the appendix as Tables 5.1, 5.2, and twelve. Which correspond to models one, two, and three respectively.

Conversion Factor (Bq/mR/hr)						
	Exposure Point					
Energy (MeV)	1	2	3	4	5	Activity (Bq)
0.015	4.87E+12	3.62E+12	3.28E+12	3.62E+12	4.87E+12	1.00E+00
0.02	1.32E+08	1.11E+08	1.05E+08	1.11E+08	1.32E+08	1.00E+00
0.03	6.93E+05	6.43E+05	6.27E+05	6.43E+05	6.93E+05	1.00E+00
0.04	2.67E+05	2.54E+05	2.50E+05	2.54E+05	2.67E+05	1.00E+00
0.05	2.36E+05	2.27E+05	2.25E+05	2.27E+05	2.36E+05	1.00E+00
0.06	2.50E+05	2.42E+05	2.40E+05	2.42E+05	2.50E+05	1.00E+00
0.08	2.64E+05	2.57E+05	2.54E+05	2.57E+05	2.64E+05	1.00E+00
0.1	2.41E+05	2.34E+05	2.31E+05	2.34E+05	2.41E+05	1.00E+00
0.15	1.99E+05	1.93E+05	1.90E+05	1.93E+05	1.99E+05	1.00E+00
0.2	1.59E+05	1.54E+05	1.52E+05	1.54E+05	1.59E+05	1.00E+00
0.3	1.08E+05	1.04E+05	1.03E+05	1.04E+05	1.08E+05	1.00E+00
0.4	8.26E+04	7.97E+04	7.87E+04	7.97E+04	8.26E+04	1.00E+00
0.5	6.74E+04	6.50E+04	6.42E+04	6.50E+04	6.74E+04	1.00E+00
0.6	5.74E+04	5.53E+04	5.46E+04	5.53E+04	5.74E+04	1.00E+00
0.8	4.54E+04	4.38E+04	4.32E+04	4.38E+04	4.54E+04	1.00E+00
1	3.78E+04	3.64E+04	3.59E+04	3.64E+04	3.78E+04	1.00E+00
1.5	2.78E+04	2.67E+04	2.64E+04	2.67E+04	2.78E+04	1.00E+00
2	2.26E+04	2.18E+04	2.15E+04	2.18E+04	2.26E+04	1.00E+00
3	1.72E+04	1.65E+04	1.63E+04	1.65E+04	1.72E+04	1.00E+00
4	1.41E+04	1.36E+04	1.34E+04	1.36E+04	1.41E+04	1.00E+00
5	1.21E+04	1.17E+04	1.15E+04	1.17E+04	1.21E+04	1.00E+00
6	1.07E+04	1.03E+04	1.01E+04	1.03E+04	1.07E+04	1.00E+00
8	8.64E+03	8.33E+03	8.22E+03	8.33E+03	8.64E+03	1.00E+00
10	7.29E+03	7.03E+03	6.94E+03	7.03E+03	7.29E+03	1.00E+00
15	5.30E+03	5.10E+03	5.04E+03	5.10E+03	5.30E+03	1.00E+00

Table 5.1 Conversion Factors for Model 1

Conversion Factor (Bq/mR/hr)						
	Exposure Point					
Energy (MeV)	1	2	3	4	5	Activity (Bq)
0.02	4.00E+03	4.13E+03	4.73E+03	7.97E+03	2.05E+04	1
0.02	5.33E+03	5.51E+03	6.30E+03	9.78E+03	1.96E+04	1
0.03	1.03E+04	1.07E+04	1.21E+04	1.78E+04	3.12E+04	1
0.04	1.66E+04	1.71E+04	1.94E+04	2.82E+04	4.83E+04	1
0.05	2.18E+04	2.24E+04	2.54E+04	3.67E+04	6.24E+04	1
0.06	2.43E+04	2.51E+04	2.83E+04	4.10E+04	6.97E+04	1
0.08	2.32E+04	2.39E+04	2.70E+04	3.92E+04	6.71E+04	1
0.10	1.95E+04	2.01E+04	2.27E+04	3.31E+04	5.71E+04	1
0.15	1.23E+04	1.27E+04	1.44E+04	2.12E+04	3.70E+04	1
0.20	8.73E+03	9.00E+03	1.02E+04	1.50E+04	2.65E+04	1
0.30	5.48E+03	5.65E+03	6.41E+03	9.47E+03	1.68E+04	1
0.40	4.03E+03	4.15E+03	4.71E+03	6.96E+03	1.24E+04	1
0.50	3.21E+03	3.31E+03	3.75E+03	5.55E+03	9.89E+03	1
0.60	2.69E+03	2.77E+03	3.15E+03	4.66E+03	8.32E+03	1
0.80	2.08E+03	2.14E+03	2.43E+03	3.60E+03	6.43E+03	1
1.00	1.71E+03	1.77E+03	2.01E+03	2.97E+03	5.31E+03	1
1.50	1.25E+03	1.29E+03	1.47E+03	2.17E+03	3.89E+03	1
2.00	1.02E+03	1.05E+03	1.20E+03	1.77E+03	3.17E+03	1
3.00	7.77E+02	8.01E+02	9.09E+02	1.35E+03	2.41E+03	1
4.00	6.39E+02	6.58E+02	7.47E+02	1.11E+03	1.98E+03	1
5.00	5.51E+02	5.68E+02	6.45E+02	9.55E+02	1.71E+03	1
6.00	4.85E+02	5.00E+02	5.67E+02	8.40E+02	1.50E+03	1
8.00	3.93E+02	4.05E+02	4.60E+02	6.81E+02	1.22E+03	1
10.00	3.32E+02	3.42E+02	3.88E+02	5.74E+02	1.03E+03	1
15.00	2.41E+02	2.48E+02	2.82E+02	4.17E+02	7.45E+02	1

Table 5.2 Conversion Factors for Model 2

Conversion Factor (Bq/mR/hr)				
	Exposure Point			
Energy (MeV)	1	2	3	Activity (Bq)
0.015	2.035E+04	2.096E+04	2.045E+04	1
0.02	1.955E+04	1.995E+04	1.960E+04	1
0.03	3.115E+04	3.166E+04	3.122E+04	1
0.04	4.819E+04	4.895E+04	4.831E+04	1
0.05	6.227E+04	6.321E+04	6.238E+04	1
0.06	6.954E+04	7.062E+04	6.969E+04	1
0.08	6.698E+04	6.798E+04	6.711E+04	1
0.1	5.701E+04	5.790E+04	5.714E+04	1
0.15	3.691E+04	3.751E+04	3.700E+04	1
0.2	2.640E+04	2.682E+04	2.646E+04	1
0.3	1.674E+04	1.702E+04	1.678E+04	1
0.4	1.235E+04	1.256E+04	1.238E+04	1
0.5	9.872E+03	1.003E+04	9.891E+03	1
0.6	8.299E+03	8.432E+03	8.319E+03	1
0.8	6.410E+03	6.519E+03	6.427E+03	1
1	5.299E+03	5.388E+03	5.311E+03	1
1.5	3.876E+03	3.940E+03	3.885E+03	1
2	3.162E+03	3.214E+03	3.169E+03	1
3	2.400E+03	2.440E+03	2.406E+03	1
4	1.973E+03	2.006E+03	1.977E+03	1
5	1.703E+03	1.731E+03	1.707E+03	1
6	1.497E+03	1.522E+03	1.500E+03	1
8	1.213E+03	1.233E+03	1.216E+03	1
10	1.024E+03	1.041E+03	1.026E+03	1
15	7.435E+02	7.559E+02	7.452E+02	1

Table 5.3 Conversion Factors for Model 3

By having these conversion factors available the amount of activity present in a wound can be estimated. Using the same collimation technique that was described above for determining wound shape under the skin, the activity deposited in a wound can be estimated by counting small portions of the wound at a time. Using a collimating material with a small hole punched through it and moving the hole in measured patterns up and down the side of the wound, as well as around the top and bottom of the wound, the activity of

small portions of the wound can be obtained. For example, using the diagram from model one, where the exposure points were placed vertically down the side of the wound with a bone shield between the wound and the exposure points, the collimating material can be moved from the first exposure point to the second, to the third, etc. and then when exposure at each point is known, the conversion factors listed in the Tables in the appendix can be used to determine activity at each of these intervals.

An important note is that the conversion factors generated through this method are model specific. This is due to the variations that occur between different counting locations. For example, a wound to the leg would have different tissue and bone thicknesses that would need to be accounted for. As a result, the creation of a single conversion factor that worked perfectly in every situation is impossible. Even if the wound is incurred in the same place but on a different person, there would still be variation in the tissue and bone thicknesses that would need to be adjusted. Even with this source of error, these conversion factors can still be used to obtain an estimate of wound activity. Once the conversion factors are applied, the activity that was picked up by the detectors is converted the initial activity that is in the actual wound. An estimate of total wound activity would be generated for each point, in order to get a more accurate estimate the activities for each point should be averaged.

Another method of determining how much activity has been deposited in a wound is through the use of a Sievert function. Sievert functions (F_s) are integrals that allow for the total wound activity to be estimated from each individual exposure point (Equation 5.1).

Equation 5.1 Sievert Function

$$F_s = \int_0^{\theta_T} e^{-\mu x \sec\theta}\, d\theta$$

The solution to the Sievert function is just one component that is needed to estimate the total activity in a wound. The rest of the factors that are needed are the measured exposure rate, the depth of the wound, the distance of the exposure point from the wound, the gamma ray yield and energy which are both nuclide specific, the mass absorption coefficient, and finally some conversion factors. All of this can be seen in Equation 5.2. When estimating activity through the use of Sievert functions, an estimate of total wound activity will be produced for each exposure point. These estimates should then be averaged to gain a final estimate. An example of how to apply this technique is shown in the next section.

Equation 5.2 Activity Calculation

$$A[Bq] = S\left[{}^{\gamma}/_{s}\right] \cdot Y\left[{}^{dis}/_{\gamma}\right] = \frac{\dot{X}\left[{}^{R}/_{s}\right] \cdot 4\pi \cdot d[cm] \cdot x[cm] \cdot \left(0.00873\ \left[{}^{J}/_{kg\ R}\right]\right) \cdot Y\left[{}^{dis}/_{\gamma}\right]}{E\left[{}^{MeV}/_{\gamma}\right] \cdot \frac{\mu_{en}}{\rho}\left[{}^{cm^2}/_{g}\right] \cdot 1.6x10^{-10}\left[{}^{J\ g}/_{MeV\ kg}\right] \int_0^{\theta_T} e^{-\mu x \sec\theta}\, d\theta}$$

An important note about this particular use of Sievert functions is that they are intended for situations where the exposure point has a full line of sight to the entirety of the line source. Unfortunately, in the case of wound counting using the previously described method with collimators, the

exposure points will not have a full line of sight on the line source. This presents another source of error in the estimation of radioactivity deposited inside a wound, which would ultimately result in an overall underestimation of wound activity. Additionally, the Sievert function assumes homogenous material composition between the exposure point and the source, which with the composition of the human body is not entirely accurate since there are multiple tissues of different densities (i.e. tissue, bone, etc.).

Chapter 6: Examples

This example is based on a suspected deposition of Cs-137 to the left hand of a worker. The wound is simulated to have occurred between the first and middle fingers of the left hand between the knuckles on the hand. The wound is assumed to be equally spaced between the two fingers, as well as between the back of the hand, and the palm of the hand, as shown in Figure 6.1. The exposure rates in this example were determined using the exposure factors generated through Microshield, and are shown in Table 6.1. This allows for the exposure estimate provided by the calculational method to be checked against the expected value.

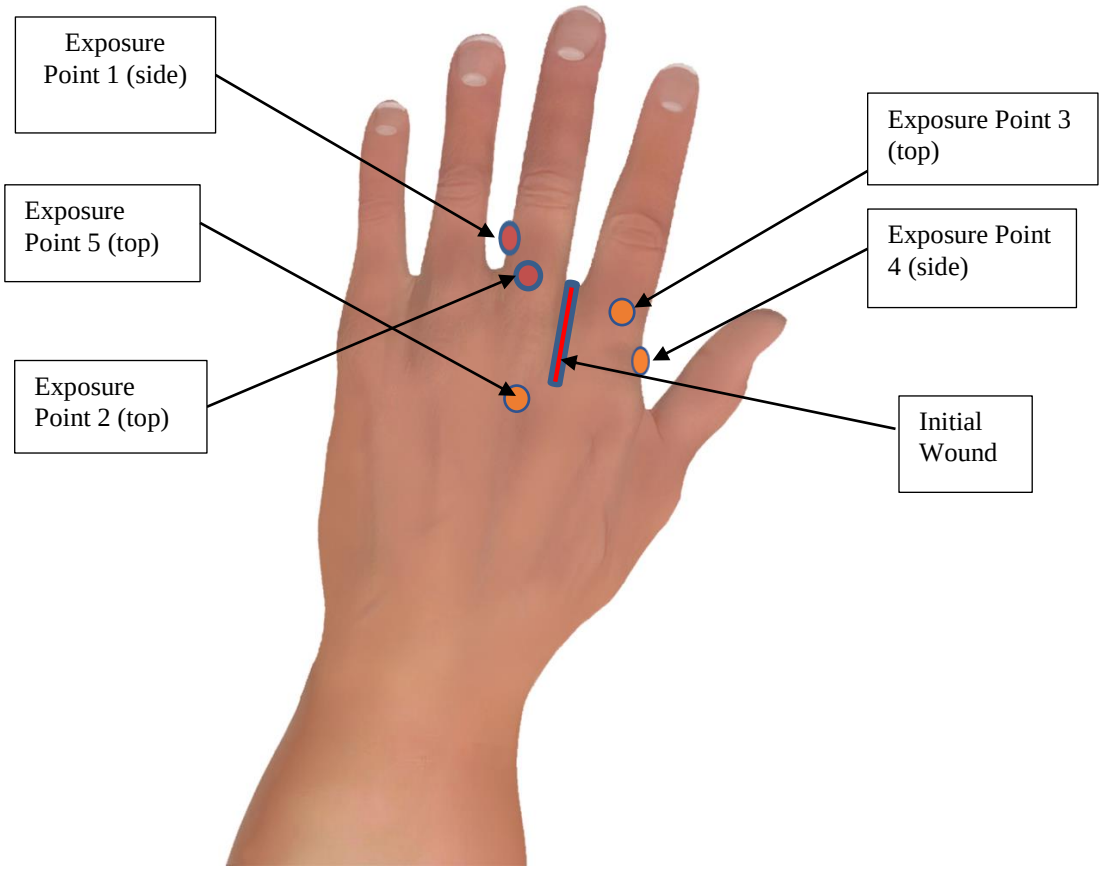

Figure 6.1 Example Wound

THIS METHOD IS TOTALLY CALCULATIONAL WITH AN ASSUMPTION OF WOUND DEPTH							
			Seivert			Estimated	
Exposure	x	θ_T	function	Exposure	Exposure	Activity	
Point	(cm)	(radians)	F_S	(mR/hr)	(R/s)	(Bq)	
1	3	0.322	0.2485	0.34	9.44E-08	3.81E+04	
2	0.9	0.838	0.7680	0.33	9.17E-08	3.59E+03	
3	0.8	0.896	0.8277	1.22	3.39E-07	1.10E+04	
4	2.6	0.367	0.2928	0.67	1.86E-07	5.53E+04	
5	2	0.464	0.3890	0.41	1.14E-07	1.96E+04	
					AVERAGE Estimated Activity (Bq):	2.55E+04	Bq

Table 6.1 Example Wound Calculations

There are two methods for estimating the activity in a wound. The first is a calculational method that uses assumptions about the wound depth and exposure points to create and then average several different estimated activities to attempt to estimate the total activity in the wound. This is the first

method that is discussed in this example. The second method is to use the exposure factors that were shown earlier to directly estimate each the activity in the wound at each point, this is the second method discussed in this example.

The data in Table 6.1 shows variables for each of the five exposure points marked in Figure 6.1. The first column lists the exposure point, the second column shows the point's distance from the source in centimeters. The third column shows the value of θ_T which is the total angle in radians. The fourth column is the solution of the Sievert Function (F_s). The Equation for the Sievert Function is shown in a repetition of Equation 5.1. The fifth column shows the hypothetical exposure rate at each point measured in milliroentgen per hour at each exposure point as shown in Figure 6.1. The next column simply converts milliroentgen per how to roentgen per second. Finally, the last column shows an estimated activity as calculated by a repetition of Equation 5.2.

Equation 5.1

$$F_s = \int_0^{\theta_T} e^{-\mu x \sec\theta}\, d\theta$$

Equation 5.2

$$A[Bq] = S\left[{}^{\gamma}/_{s}\right] \cdot Y\left[{}^{dis}/_{\gamma}\right] = \frac{\dot{X}\left[{}^{R}/_{s}\right] \cdot 4\pi \cdot d[cm] \cdot x[cm] \cdot \left(0.00873\ \left[{}^{J}/_{kg\ R}\right]\right) \cdot Y\left[{}^{dis}/_{\gamma}\right]}{E\left[{}^{MeV}/_{\gamma}\right] \cdot \frac{\mu_{en}}{\rho}\left[{}^{cm^2}/_{g}\right] \cdot 1.6x10^{-10}\left[{}^{J\ g}/_{MeV\ kg}\right] \int_0^{\theta_T} e^{-\mu x \sec\theta}\, d\theta}$$

The Sievert function was used as a summation tool to estimate the total wound activity as measured at each individual point. This was chosen over other methods of modelling (such as MCNP) because a Table of Sievert values can be constructed with relative ease, and then quickly consulted in the event of a radiologically contaminated wound. Whereas using MCNP would require knowledge and experience with the software in order to effectively build the model.

Where $\dot{X}$ is representative of the exposure rate in Roentgen per second, d is the depth of the wound in centimeters (which is the same for all exposure points), x is the distance of the exposure point from the source (wound) in centimeters, and Y is the yield of disintegrations resulting in a gamma being emitted. For the denominator, E is the energy of the photon (.662 MeV in this case), $\frac{\mu_{en}}{\rho}$ is the mass attenuation coefficient, and the last term in the numerator is the Sievert Function. The values for wound depth, the value of mu in tissue, photon energy/yield, and the conversion factors can be seen in Table 6.2.

assumed wound depth in cm (d):	1	cm
μ_{en}/ρ in air (cm^2/g):	0.0293	cm^2/g
μ in tissue (cm^-1):	0.0849	cm^{-1}
photon energy in MeV (E):	0.662	MeV
photon yield (Y):	0.946	
conversion (J/kg*R):	0.00873	J/kg*R
conversion (J*g/MeV*kg):	1.60E-10	J*g/MeV*kg

Table 6.2 Constants for Example Wound

The calculations for this example were performed in Microsoft Excel, each value was entered into a Table, and then referenced in each of the five different exposure point calculations in order to reduce the potential error from entering each value multiple times. Once the estimated activity for each of the five exposure points was calculated, the numbers were averaged. This is because each individual calculation is itself an estimate of the total activity in the wound. Another important note about this method of estimating wound activity is that it is based on assumptions like how far the exposure point is from the wound, how deep the wound is, etc. This results in a variation occurring in calculations on the same wound due simply to different assumptions being made by the various users.

The second method of estimating total activity in the wound is to take the measured exposure rates and divide them by the exposure factors from the Microshield models. This method is shown in Table 6.3.

Exposure Point	Exposure (mR/hr)	Exposure Factor (mR/hr per Bq)	Activity (Bq)
1	0.34	9.2E-06	3.70E+04
2	0.33	8.9E-06	3.71E+04
3	1.22	3.3E-05	3.70E+04
4	0.67	1.8E-05	3.72E+04
5	0.41	1.1E-05	3.73E+04
	Average Activity (Bq):		3.71E+04

Table 6.3 Activity Calculate from Conversion Factors

As with the first method, the estimated activities for each exposure point should be averaged together because each one is itself an estimate of the total activity deposited in a wound. Something to notice about these two

methods is that they will result in different answers. The first method, using the Equations to calculate the activity based on the exposure rates does not take attenuation due to bone into account while the exposure factors generated using Microshield do. This difference in approach helps to explain the difference in the estimated activities.

Chapter 7: Conclusion

The Microshield simulations show a dependence of exposure rates on the position of the exposure points relative to the cylindrical source, when the source is oriented straight up and down. When the source is oriented in a vertical position, the exposure rates at the points that run parallel to the source remain fairly constant. When the exposure points are oriented perpendicular to the source, the exposure rates drop off as the points get further from the center of the puncture. If the exposure points are distributed in an arc around the puncture, they will give the same results unless the puncture is not oriented in a vertical fashion. All of this information could be used to locate activity in a wound, and to gain more information about what the wound looks like under the surface of the skin.

The technique of using a collimator and moving it around to take multiple counts from various sides and distances of a wound would help increase the understanding of the wound. The facilities at the In-Vivo Radiobioassay Research Facility would be an ideal place to apply this technique. The heavily shielded counting cells at the IVRRF would help to

reduce the impact of background radiation, which in turn would help increase the accuracy of the triangulation.

As was shown in the examples section, when applied, the calculational method of using Sievert functions results in an estimate of total wound activity, but this is an estimate only. The activity numbers shown in the example are lower than the activity that was used to plan the example through the conversion factors. An explanation of this is that the Sievert function only takes into account the attenuation of photons due to tissue, and does not include an estimate for attenuation due to bone. The conversion factors that were generated with Microshield take both bone and tissue attenuation into account, which would justify the difference between results gathered from the two methods.

To gain an even better understanding of radiation wounds, a model or phantom could be created. Creating a physical model of the hand, or any other body part of interest, would be helpful in applying this technique and investigating the complex methodologies behind radiation wound counting.

The creation of a physical model or phantom would be a rather difficult task. Creating a physical representation of any body part is relatively easy, the difficulty comes in making sure it is representative of the population that the computer models would be applied to. This is a very hard thing to do because, especially with extremities, since there is a large variation in the population.

Chapter 7: References

1. Alikhani, L. (2014, June 20). First Look Into Rooms Where Hanford Workers are Tested for Levels of radioactive materials in the Body. Retrieved August 08, 2017, from http://www.yaktrinews.com/news/first-look-rooms-where-hanford-workers-are-tested-/362397083
2. Baes, F. (n.d.). Buildup Factor. Retrieved October 06, 2017, from http://hps.org/publicinformation/radterms/radfact161.html
3. Bailey, B. R., Eckerman, K. F., & Townsend, L. W. (2003). An Analysis of a Puncture Wound Case with Medical Intervention. Radiation Protection Dosimetry, 105, 509-512. Retrieved August 28, 2017.
4. Carbaugh, E. H. (1994). Practical Applications of Internal Dose Calculations. In Internal Radiation Dosimetry (pp. 529-542). Madison, WI: Medical Physics Publishing.
5. Carbaugh, E. H., Lynch, T. P., Antonio, C. L., & Valle, F. M. (2010). Twenty-Four Years of Follow-Up for a Hanford Plutonium Wound Case (pp. 483-494, Tech.). Health Physics Society. doi:10.1097/HP.0b013e3181d96381
6. Cember, H., & Johnson, T. E. (2009). Introduction to health physics (4th ed.). New York: McGraw-Hill.
7. Collimator. (2017, July 29). Retrieved August 08, 2017, from https://en.wikipedia.org/wiki/Collimator
8. Griffiths, N. M., Coudert, S., Renault, D., Wilk, J., & Van der Meeren, A. (2014). Actinide Handling After Wound Entry with Local or Systemic Decorporation Therapy in the Rat. International Journal of Radiation Biology, 989-995. Retrieved August 28, 2017.
9. Hall, E. J., & Giaccia, A. J. (2012). Radiobiology for the radiologist (7th ed.). Philadelphia, Pa. etc.: Wolters Kluwer Health.
10. Hickman, D. P. (2006). Errors Associated with the Direct Measurement of Radionuclides in Wounds (pp. 1-10, Tech.). Livermore, CA: Lawrence Livermore National Laboratory.
11. Ishigure, N. (2009). Implementation of the NCRP Wound Model for Interpretation of Bioassay Data for Intake of Radionuclides Through Contaminated Wounds. Journal of Radiation Research, 50(3), 267-276. doi:10.1269/jrr.09004
12. Jolly, L., Jr., McClearen, H. A., Poda, G. A., & Walke, W. P. (1972). Treatment and Evaluation of a Plutonium-238 Nitrate Contaminated Puncture Wound (Vol. 23, pp. 333-341, Tech.). Pergamon Press.
13. Jones, E., & Saxby, W. (1968). The Detection And Measurement Of Plutonium Contamination In Wounds. Proceedings of the First International Congress of Radiation Protection, 1295-1307. doi:10.1016/b978-1-4832-8312-8.50193-4
14. Kirby, J. A., Anspaugh, L. R., Phelps, P. L., Juckabay, G. W., Markwell, F., & Barnes, M. (1977). A comparison of in-situ gamma soil analysis and soil sampling data for mapping 241 Am and 239 Pu Soil Concentrations at the Nevada Test Site. IEEE Transactions on Nuclear Science, 587-589. Retrieved June, 2017.
15. Lynch, T. P., & Carbaugh, E. H. (2017, August 3). Thesis Research [E-mail to the author].
16. Schadilov, A. E., Belosokhov, M. V., & Levina, E. S. (2010). A Case of Wound Intake of Plutonium Isotopes and 241 Am in a Human: Application and Improvement of the NCRP Wound Model. Health Physics, 99(4), 560-567. Retrieved August 28, 2017.
17. Tassani, S., Ohman, C., Baruffaldi, F., Baleani, M., & Viceconti, M. (2010). Volume to Density Relation in Adult Human Bone Tissue. Journal of Biomechanics. Retrieved August 28, 2017.
    (Tassani, Ohman, Baruffaldi, Baleani &Viceconti, 2010)
18. Turner, J. E. (2007). Atoms, radiation, and radiation protection. Weinheim: Wiley-VCH.

19. Vorvick, L. J. (2015, August 14). Long bones. Retrieved October 06, 2017, from https://medlineplus.gov/ency/imagepages/9582.htm
20. Weber, W., Doyle-Eisele, M., Seilkop, S. K., & Guilmette, R. (2012). Biokinetics of Systemically Distributed Co-60 in the Rat: An Experimental Model Useful in Evaluating Medical Countermeasures for Internal Contamination. Health Physics, 103(4), 474-483. Retrieved August 28, 2017.
21. Young, A., & Mcnaught, C. (2011). The Physiology of Wound Healing. Surgery, 29(10), 475-479. Retrieved September 14, 2017.

Appendices

Exposure Rate with Buildup (mR/hr)						
	Exposure Point					
Energy (MeV)	1	2	3	4	5	Activity (Bq)
0.015	2.05E-13	2.76E-13	3.05E-13	2.76E-13	2.05E-13	1.00E+00
0.02	7.59E-09	8.97E-09	9.49E-09	8.97E-09	7.59E-09	1.00E+00
0.03	1.44E-06	1.56E-06	1.59E-06	1.56E-06	1.44E-06	1.00E+00
0.04	3.75E-06	3.93E-06	4.00E-06	3.93E-06	3.75E-06	1.00E+00
0.05	4.24E-06	4.40E-06	4.45E-06	4.40E-06	4.24E-06	1.00E+00
0.06	4.00E-06	4.13E-06	4.18E-06	4.13E-06	4.00E-06	1.00E+00
0.08	3.78E-06	3.90E-06	3.94E-06	3.90E-06	3.78E-06	1.00E+00
0.1	4.15E-06	4.28E-06	4.32E-06	4.28E-06	4.15E-06	1.00E+00
0.15	5.03E-06	5.19E-06	5.25E-06	5.19E-06	5.03E-06	1.00E+00
0.2	6.29E-06	6.51E-06	6.59E-06	6.51E-06	6.29E-06	1.00E+00
0.3	9.30E-06	9.63E-06	9.75E-06	9.63E-06	9.30E-06	1.00E+00
0.4	1.21E-05	1.26E-05	1.27E-05	1.26E-05	1.21E-05	1.00E+00
0.5	1.48E-05	1.54E-05	1.56E-05	1.54E-05	1.48E-05	1.00E+00
0.6	1.74E-05	1.81E-05	1.83E-05	1.81E-05	1.74E-05	1.00E+00
0.8	2.20E-05	2.29E-05	2.32E-05	2.29E-05	2.20E-05	1.00E+00
1	2.65E-05	2.75E-05	2.78E-05	2.75E-05	2.65E-05	1.00E+00
1.5	3.60E-05	3.74E-05	3.79E-05	3.74E-05	3.60E-05	1.00E+00
2	4.42E-05	4.59E-05	4.65E-05	4.59E-05	4.42E-05	1.00E+00
3	5.82E-05	6.05E-05	6.12E-05	6.05E-05	5.82E-05	1.00E+00
4	7.10E-05	7.37E-05	7.46E-05	7.37E-05	7.10E-05	1.00E+00
5	8.24E-05	8.55E-05	8.66E-05	8.55E-05	8.24E-05	1.00E+00
6	9.39E-05	9.74E-05	9.87E-05	9.74E-05	9.39E-05	1.00E+00
8	1.16E-04	1.20E-04	1.22E-04	1.20E-04	1.16E-04	1.00E+00
10	1.37E-04	1.42E-04	1.44E-04	1.42E-04	1.37E-04	1.00E+00
15	1.89E-04	1.96E-04	1.99E-04	1.96E-04	1.89E-04	1.00E+00

Table 1: Exposure Rates (mR/hr) for side bone shield and side exposure points (Model 1)

position (cm)	1	2	3	4	5
x	2.25	2.25	2.25	2.25	2.25
y	0	0.25	0.5	0.75	1
z	0	0	0	0	0

Table 2: Exposure Point Positions for side bone shield and side exposure points (Model 1)

Point	Total Exposure
1	9.618E-04
2	9.984E-04
3	1.011E-03
4	9.984E-04
5	9.618E-04
Total	4.931E-03

Table 3: Total Exposure Rates for side bone shield and side exposure points (Model 1)

Conversion Factor (Bq/mR/hr)						
	Exposure Point					
Energy (MeV)	1	2	3	4	5	Activity (Bq)
0.015	4.87E+12	3.62E+12	3.28E+12	3.62E+12	4.87E+12	1.00E+00
0.02	1.32E+08	1.11E+08	1.05E+08	1.11E+08	1.32E+08	1.00E+00
0.03	6.93E+05	6.43E+05	6.27E+05	6.43E+05	6.93E+05	1.00E+00
0.04	2.67E+05	2.54E+05	2.50E+05	2.54E+05	2.67E+05	1.00E+00
0.05	2.36E+05	2.27E+05	2.25E+05	2.27E+05	2.36E+05	1.00E+00
0.06	2.50E+05	2.42E+05	2.40E+05	2.42E+05	2.50E+05	1.00E+00
0.08	2.64E+05	2.57E+05	2.54E+05	2.57E+05	2.64E+05	1.00E+00
0.1	2.41E+05	2.34E+05	2.31E+05	2.34E+05	2.41E+05	1.00E+00
0.15	1.99E+05	1.93E+05	1.90E+05	1.93E+05	1.99E+05	1.00E+00
0.2	1.59E+05	1.54E+05	1.52E+05	1.54E+05	1.59E+05	1.00E+00
0.3	1.08E+05	1.04E+05	1.03E+05	1.04E+05	1.08E+05	1.00E+00
0.4	8.26E+04	7.97E+04	7.87E+04	7.97E+04	8.26E+04	1.00E+00
0.5	6.74E+04	6.50E+04	6.42E+04	6.50E+04	6.74E+04	1.00E+00
0.6	5.74E+04	5.53E+04	5.46E+04	5.53E+04	5.74E+04	1.00E+00
0.8	4.54E+04	4.38E+04	4.32E+04	4.38E+04	4.54E+04	1.00E+00
1	3.78E+04	3.64E+04	3.59E+04	3.64E+04	3.78E+04	1.00E+00
1.5	2.78E+04	2.67E+04	2.64E+04	2.67E+04	2.78E+04	1.00E+00
2	2.26E+04	2.18E+04	2.15E+04	2.18E+04	2.26E+04	1.00E+00
3	1.72E+04	1.65E+04	1.63E+04	1.65E+04	1.72E+04	1.00E+00
4	1.41E+04	1.36E+04	1.34E+04	1.36E+04	1.41E+04	1.00E+00
5	1.21E+04	1.17E+04	1.15E+04	1.17E+04	1.21E+04	1.00E+00
6	1.07E+04	1.03E+04	1.01E+04	1.03E+04	1.07E+04	1.00E+00
8	8.64E+03	8.33E+03	8.22E+03	8.33E+03	8.64E+03	1.00E+00
10	7.29E+03	7.03E+03	6.94E+03	7.03E+03	7.29E+03	1.00E+00
15	5.30E+03	5.10E+03	5.04E+03	5.10E+03	5.30E+03	1.00E+00

Table 4: Conversion factors (Bq/mR) for side bone shield and side exposure points (Model 1)

Exposure Rate with Buildup (mR/hr)					
	Exposure Point				
Energy (MeV)	1	2	3	4	5
0.015	2.50E-04	2.42E-04	2.12E-04	1.26E-04	4.89E-05
0.02	1.88E-04	1.82E-04	1.59E-04	1.02E-04	5.10E-05
0.03	9.67E-05	9.39E-05	8.28E-05	5.63E-05	3.20E-05
0.04	6.01E-05	5.83E-05	5.16E-05	3.55E-05	2.07E-05
0.05	4.59E-05	4.46E-05	3.94E-05	2.72E-05	1.60E-05
0.06	4.11E-05	3.99E-05	3.53E-05	2.44E-05	1.44E-05
0.08	4.31E-05	4.19E-05	3.70E-05	2.55E-05	1.49E-05
0.1	5.14E-05	4.98E-05	4.40E-05	3.02E-05	1.75E-05
0.15	8.10E-05	7.86E-05	6.94E-05	4.73E-05	2.70E-05
0.2	1.15E-04	1.11E-04	9.80E-05	6.66E-05	3.78E-05
0.3	1.82E-04	1.77E-04	1.56E-04	1.06E-04	5.96E-05
0.4	2.48E-04	2.41E-04	2.12E-04	1.44E-04	8.08E-05
0.5	3.12E-04	3.03E-04	2.67E-04	1.80E-04	1.01E-04
0.6	3.72E-04	3.60E-04	3.18E-04	2.15E-04	1.20E-04
0.8	4.82E-04	4.67E-04	4.12E-04	2.78E-04	1.56E-04
1	5.83E-04	5.66E-04	4.98E-04	3.36E-04	1.88E-04
1.5	7.98E-04	7.74E-04	6.82E-04	4.60E-04	2.57E-04
2	9.78E-04	9.49E-04	8.36E-04	5.64E-04	3.16E-04
3	1.29E-03	1.25E-03	1.10E-03	7.43E-04	4.16E-04
4	1.57E-03	1.52E-03	1.34E-03	9.03E-04	5.06E-04
5	1.81E-03	1.76E-03	1.55E-03	1.05E-03	5.86E-04
6	2.06E-03	2.00E-03	1.76E-03	1.19E-03	6.67E-04
8	2.55E-03	2.47E-03	2.18E-03	1.47E-03	8.23E-04
10	3.02E-03	2.93E-03	2.58E-03	1.74E-03	9.75E-04
15	4.15E-03	4.03E-03	3.55E-03	2.40E-03	1.34E-03

Table 5: Exposure Rates (mR/hr) for top exposure points arranged in linear fashion (Model 2)

position (cm)	1	2	3	4	5
x	0	0.2	0.4	0.6	0.8
y	1.01	1.01	1.01	1.01	1.01
z	0	0	0	0	0

Table 6: Exposure Point Positions for top exposure points arranged in linear fashion (Model 2)

Point	Total Exposure
1	2.14E-02
2	2.07E-02
3	1.83E-02
4	1.23E-02
5	6.87E-03

Table 7: Total Exposure (mR/hr) and Dose (Gy/hr) Rates for top exposure points arranged in linear fashion (Model 2)

Conversion Factor (Bq/mR/hr)						
	Exposure Point					
Energy (MeV)	1	2	3	4	5	Activity (Bq)
0.02	4.00E+03	4.13E+03	4.73E+03	7.97E+03	2.05E+04	1
0.02	5.33E+03	5.51E+03	6.30E+03	9.78E+03	1.96E+04	1
0.03	1.03E+04	1.07E+04	1.21E+04	1.78E+04	3.12E+04	1
0.04	1.66E+04	1.71E+04	1.94E+04	2.82E+04	4.83E+04	1
0.05	2.18E+04	2.24E+04	2.54E+04	3.67E+04	6.24E+04	1
0.06	2.43E+04	2.51E+04	2.83E+04	4.10E+04	6.97E+04	1
0.08	2.32E+04	2.39E+04	2.70E+04	3.92E+04	6.71E+04	1
0.10	1.95E+04	2.01E+04	2.27E+04	3.31E+04	5.71E+04	1
0.15	1.23E+04	1.27E+04	1.44E+04	2.12E+04	3.70E+04	1
0.20	8.73E+03	9.00E+03	1.02E+04	1.50E+04	2.65E+04	1
0.30	5.48E+03	5.65E+03	6.41E+03	9.47E+03	1.68E+04	1
0.40	4.03E+03	4.15E+03	4.71E+03	6.96E+03	1.24E+04	1
0.50	3.21E+03	3.31E+03	3.75E+03	5.55E+03	9.89E+03	1
0.60	2.69E+03	2.77E+03	3.15E+03	4.66E+03	8.32E+03	1
0.80	2.08E+03	2.14E+03	2.43E+03	3.60E+03	6.43E+03	1
1.00	1.71E+03	1.77E+03	2.01E+03	2.97E+03	5.31E+03	1
1.50	1.25E+03	1.29E+03	1.47E+03	2.17E+03	3.89E+03	1
2.00	1.02E+03	1.05E+03	1.20E+03	1.77E+03	3.17E+03	1
3.00	7.77E+02	8.01E+02	9.09E+02	1.35E+03	2.41E+03	1
4.00	6.39E+02	6.58E+02	7.47E+02	1.11E+03	1.98E+03	1
5.00	5.51E+02	5.68E+02	6.45E+02	9.55E+02	1.71E+03	1
6.00	4.85E+02	5.00E+02	5.67E+02	8.40E+02	1.50E+03	1
8.00	3.93E+02	4.05E+02	4.60E+02	6.81E+02	1.22E+03	1
10.00	3.32E+02	3.42E+02	3.88E+02	5.74E+02	1.03E+03	1
15.00	2.41E+02	2.48E+02	2.82E+02	4.17E+02	7.45E+02	1

Table 8: Conversion Factors (Bq/mR) for Top Exposure Points Arranged in Linear Fashion (Model 2)

Exposure Rate with Buildup (mR/hr)			
	Exposure Point		
Energy (MeV)	1	2	3
0.015	4.915E-05	4.772E-05	4.889E-05
0.02	5.114E-05	5.012E-05	5.101E-05
0.03	3.210E-05	3.159E-05	3.203E-05
0.04	2.075E-05	2.043E-05	2.070E-05
0.05	1.606E-05	1.582E-05	1.603E-05
0.06	1.438E-05	1.416E-05	1.435E-05
0.08	1.493E-05	1.471E-05	1.490E-05
0.1	1.754E-05	1.727E-05	1.750E-05
0.15	2.709E-05	2.666E-05	2.703E-05
0.2	3.788E-05	3.728E-05	3.780E-05
0.3	5.972E-05	5.876E-05	5.959E-05
0.4	8.095E-05	7.964E-05	8.077E-05
0.5	1.013E-04	9.969E-05	1.011E-04
0.6	1.205E-04	1.186E-04	1.202E-04
0.8	1.560E-04	1.534E-04	1.556E-04
1	1.887E-04	1.856E-04	1.883E-04
1.5	2.580E-04	2.538E-04	2.574E-04
2	3.163E-04	3.111E-04	3.156E-04
3	4.166E-04	4.098E-04	4.157E-04
4	5.069E-04	4.986E-04	5.057E-04
5	5.873E-04	5.777E-04	5.859E-04
6	6.680E-04	6.571E-04	6.665E-04
8	8.246E-04	8.111E-04	8.227E-04
10	9.770E-04	9.610E-04	9.747E-04
15	1.345E-03	1.323E-03	1.342E-03

Table 9: Exposure Rates (mR/hr) for for top exposure points in semi-circle (model 3)

position (cm)	1	2	3
x	0	0.57	0.8
y	1.01	1.01	1.01
z	0.8	0.57	0

Table 10: Exposure Point Positions for top exposure points in semi-circle (model 3)

Point	Total Exposure
1	6.89E-03
2	6.78E-03
3	6.87E-03

Table 11: Total Exposure (mR/hr) and Dose (Gy/hr) rates for top exposure points in semi-circle (model 3)

Conversion Factor (Bq/mR/hr)				
	Exposure Point			
Energy (MeV)	1	2	3	Activity (Bq)
0.015	2.035E+04	2.096E+04	2.045E+04	1
0.02	1.955E+04	1.995E+04	1.960E+04	1
0.03	3.115E+04	3.166E+04	3.122E+04	1
0.04	4.819E+04	4.895E+04	4.831E+04	1
0.05	6.227E+04	6.321E+04	6.238E+04	1
0.06	6.954E+04	7.062E+04	6.969E+04	1
0.08	6.698E+04	6.798E+04	6.711E+04	1
0.1	5.701E+04	5.790E+04	5.714E+04	1
0.15	3.691E+04	3.751E+04	3.700E+04	1
0.2	2.640E+04	2.682E+04	2.646E+04	1
0.3	1.674E+04	1.702E+04	1.678E+04	1
0.4	1.235E+04	1.256E+04	1.238E+04	1
0.5	9.872E+03	1.003E+04	9.891E+03	1
0.6	8.299E+03	8.432E+03	8.319E+03	1
0.8	6.410E+03	6.519E+03	6.427E+03	1
1	5.299E+03	5.388E+03	5.311E+03	1
1.5	3.876E+03	3.940E+03	3.885E+03	1
2	3.162E+03	3.214E+03	3.169E+03	1
3	2.400E+03	2.440E+03	2.406E+03	1
4	1.973E+03	2.006E+03	1.977E+03	1
5	1.703E+03	1.731E+03	1.707E+03	1
6	1.497E+03	1.522E+03	1.500E+03	1
8	1.213E+03	1.233E+03	1.216E+03	1
10	1.024E+03	1.041E+03	1.026E+03	1
15	7.435E+02	7.559E+02	7.452E+02	1

Table 12: Conversion Factors (Bq/mR) for top exposure points in semi-circle (model 3)